UC Irvine
UC Irvine Previously Published Works

Title

Bidirectional global spontaneous network activity precedes the canonical unidirectional circuit organization in the developing hippocampus

Permalink

https://escholarship.org/uc/item/3tn5m853

Journal

The Journal of Comparative Neurology, 522(9)

ISSN

1550-7149

Authors

Shi, Yulin
Ikrar, Taruna
Olivas, Nicholas D
et al.

Publication Date

2014-06-15

DOI

10.1002/cne.23528

Copyright Information

Peer reviewed

Bidirectional Global Spontaneous Network Activity Precedes the Canonical Unidirectional Circuit Organization in the Developing Hippocampus

Yulin Shi,[1] Taruna Ikrar,[1] Nicholas D. Olivas,[1] and Xiangmin Xu[1,2]*

[1]Department of Anatomy and Neurobiology, School of Medicine, University of California, Irvine, California 92697-1275
[2]Department of Biomedical Engineering, University of California, Irvine, California 92697-2715

ABSTRACT

Spontaneous network activity is believed to sculpt developing neural circuits. Spontaneous giant depolarizing potentials (GDPs) were first identified with single-cell recordings from rat CA3 pyramidal neurons, but here we identify and characterize a large-scale spontaneous network activity we term *global network activation* (GNA) in the developing mouse hippocampal slices, which is measured macroscopically by fast voltage-sensitive dye imaging. The initiation and propagation of GNA in the mouse is largely GABA-independent and dominated by glutamatergic transmission via AMPA receptors. Despite the fact that signal propagation in the adult hippocampus is strongly unidirectional through the canonical trisynaptic circuit (dentate gyrus [DG] to CA3 to CA1), spontaneous GNA in the developing hippocampus originates in distal CA3 and propagates both forward to CA1 and backward to DG. Photostimulation-evoked GNA also shows prominent backward propagation in the developing hippocampus from CA3 to DG. Mouse GNA is strongly correlated to electrophysiological recordings of highly localized single-cell and local field potential events. Photostimulation mapping of neural circuitry demonstrates that the enhancement of local circuit connections to excitatory pyramidal neurons occurs over the same time course as GNA and reveals the underlying pathways accounting for GNA backward propagation from CA3 to DG. The disappearance of GNA coincides with a transition to the adult-like unidirectional circuit organization at about 2 weeks of age. Taken together, our findings strongly suggest a critical link between GNA activity and maturation of functional circuit connections in the developing hippocampus. J. Comp. Neurol. 522:2191–2208, 2014.

INDEXING TERMS: imaging; photostimulation; development

The hippocampal circuit underlies learning and memory processes and mediates pathological conditions such as temporal lobe epilepsy. The hippocampus has a distinctive trisynaptic organization that is strongly feedforward in the directionality of its information flow (i.e., dentate gyrus, DG→CA3→CA1), which contributes to both normal function and pathology. There have been considerable efforts to understand the developmental processes that lead to the adult hippocampal circuit organization. Spontaneous activity in many developing neural circuits, including the hippocampus, contributes to circuit formation. In the early developing hippocampus, GABA actions are depolarizing and excitatory, coinciding with spontaneous-recurring network events termed *giant depolarizing potentials* (GDPs; Ben-Ari et al., 1989, 2007). GDPs were initially identified with single-cell recordings from CA3 pyramidal neurons in slices of neonatal rats; further studies have continued mostly in

rat hippocampal preparations with single-cell and local field electrophysiological recordings and Ca^{2+} imaging methods (Ben-Ari et al., 1989; Bonifazi et al., 2009; Garaschuk et al., 1998; Leinekugel et al., 1997, 1998).

Propagating network events related to GDPs also have been examined by using fast voltage-sensitive dye imaging in rat hippocampal slices (Bolea et al., 2006). GDPs are believed to be GABA dependent events mediated by $GABA_A$ receptor transmission (Ben-Ari, 2002; Ben-Ari et al., 1997, 2007; but see Bolea et al., 1999; Sipila et al., 2005; Xie et al., 1994). As with GDPs observed in vitro, spontaneous sharp waves (SPWs) visible in extracellular field potential recordings have been observed in the hippocampus of neonatal and adult rats in vivo (Buhl and Buzsaki, 2005; Buzsaki, 1986; Leinekugel et al., 2002); some of these researchers suggest that SPWs and GDPs are essentially the same phenomena measured under different experimental conditions. GDPs or SPWs recorded at the microscopic level indicate that spontaneous activity is important for developing hippocampus; however, studies to date have not provided a macroscopic network-level view of the spatial and temporal dynamics of spontaneous activity or addressed the relative timing compared with the development of mature circuit connectivity.

To provide a macroscopic global view of these processes in developing hippocampus, we combined fast voltage-sensitive dye (VSD) imaging of neuronal activity and laser photostimulation by the uncaging of neurotransmitters to examine the developing circuit activity and connections in slice preparations of mouse hippocampus. This approach allows for high spatiotemporal-resolution imaging of the entire circuit, including the dentate gyrus (DG), CA3, and CA1, along with functional mapping of circuit connections. Here we describe spontaneous global network activation (GNA) measured by VSD imaging, which propagates from distal CA3 to DG as well as to CA1 in the trisynaptic circuitry. Spontaneous and evoked mouse GNAs have similar spatiotemporal properties as assessed by VSD imaging and laser photostimulation in the developing circuitry. Bidirectional GNA precedes the maturation of the mouse hippocampal circuit, insofar as GNA disappears immediately before the emergence of the unidirectional trisynaptic circuit organization that characterizes adult hippocampus.

MATERIALS AND METHODS
Slice Preparation and Experimental Conditions

All animals were handled and experiments were conducted in accordance with procedures approved by the Institutional Animal Care and Use Committee at the University of California, Irvine. Seventy-five C57/B6-background mouse pups (either sex) of postnatal day 1 (P1) to P18 were used for the experiments.

Hippocampal slices 400 μm thick were cut at the angle optimized to conserve the intrahippocampal axo-nal projections (Bischofberger et al., 2006), in well-oxygenated (95% O_2−5% CO_2), ice-cold sucrose-containing cutting solution (in mM: 85 NaCl, 75 sucrose, 2.5 KCl, 25 glucose, 1.25 NaH_2PO_4, 4 $MgCl_2$, 0.5 $CaCl_2$, and 24 $NaHCO_3$) or in artificial cerebrospinal fluid (ACSF; in mM: 126 NaCl, 2.5 KCl, 26 $NaHCO_3$, 2 $CaCl_2$, 2 $MgCl_2$, 1.25 NaH_2PO_4, and 10 glucose) with a broad-spectrum excitatory amino acid antagonist, kynurenic acid (0.2 mM). On average, one or two morphological intact slices (as illustrated at the horizontal plates 147–150 of Paxinos and Franklin, 2001) between dorsal and ventral hippocampus from each hemisphere was used for experiments. For VSD imaging experiments, slices were first incubated in the cutting solution for 30 minutes at 32°C and then transferred for dye staining at room temperature (22°C) for 1 hour in oxygenated ACSF containing 0.12 mg/ml of the absorption voltage-sensitive dye NK3630 (Kankoh-Shikiso Kenkyusho Co., Japan), then maintained in regular ACSF before use. We used standard open recording chambers, which maintained slice health and viability well, as evidenced by measurement of GNA activity for periods lasting more than 6 hours. Most imaging experiments were conducted at room temperature. Further experiments were conducted at 32°C with an in-line solution heater (Warner Instruments, Hamden, CT). The characteristics of spontaneous and evoked network activity did not differ at different temperatures. The data obtained were pooled together for analysis.

Voltage-sensitive dye imaging

Our overall system of electrophysiological recordings, photostimulation, and imaging was described previously (Xu et al., 2010). Unless otherwise specified, optical recording of VSD signals was performed under the 4× objective with a sampling rate of 4.4 msec per frame (frame resolution 88 [w] × 60 [h] pixels). The field of view covered the area of 1.28 × 1.07 mm^2 with a spatial resolution of 14.6 × 17.9 $μm^2$/pixel. To image spontaneous network activity, five to 10 sessions (nine trials per session) were conducted with 3 minutes of off-illumination intervals between sessions. For each trial, the VSD imaging duration was 2,000 frames (i.e., 8.8 seconds) with an intertrial interval of 12 seconds (i.e., 8.8 seconds for data recording plus 3.2 seconds for saving data). Each session lasted for 9 × 12 seconds (108 seconds total). With the known concern of dye phototoxicity from prolonged illumination, we chose not to image stained slices continuously and instead used spaced sessions to detect GNA events for a total duration of up to 18 minutes, which is sufficient in terms of total acquisition times. We measured the total GNA events from all these sessions against the total

imaging time to derive the GNA frequency (events per minute). For the imaging of photostimulation-evoked activity, MNI-caged glutamate (Tocris Bioscience, Ellisville, MO) or CNB-caged GABA (Invitrogen, Carlsbad, CA) was added to the ACSF at 0.2 mM. A UV laser unit (DPSS Lasers, Santa Clara, CA) was used to generate 355-nm pulses (e.g., 1 msec, 20 mW) for glutamate or GABA uncaging. VSD imaging of photostimulation-evoked activity was triggered and synchronized with laser photostimulation.

VSD signal amplitudes were originally measured by the percentage change in pixel light intensity ($\Delta I/I\%$), and expressed as standard deviation (SD) multiples above the mean baseline signal for display and quantification. The activated pixel was empirically defined as the pixel with the amplitude ≥ 1 SD above the baseline (equivalent to the detectable signal level in the original VSD maps of $\Delta I/I\%$). VSD images were smoothed by convolution with a Gaussian spatial filter (kernel size 5 pixels, standard deviation [σ] 1 pixel) and a Gaussian temporal filter (kernel size 3 frames, σ 1 frame). In the present study, single-trial VSD signals were of sufficiently high amplitudes and could be discerned from background noise; no averaging over multiple trials was used for data presentation unless specified. Images were displayed and analyzed in custom-made MATLAB programs. To quantify VSD response strength of spontaneous or photostimulation-evoked GNA, the average number of activated pixels and average response amplitude within the defined window of analysis were measured for each trial.

We follow the basic nomenclature of Lorente de Nó (1934) and Ishizuka et al. (1990) for hippocampal subfields. We do not distinguish the CA2 region because it is not well defined in early postnatal hippocampal slices (Grove and Tole, 1999; Tole et al., 1997); however, the presumptive CA2 identified in some slices appears to be part of the GNA initiation zone. The terms of proximal (nearer the dentate gyrus) and distal (farther from the dentate gyrus) are used to designate positions along the transverse axis of CA3 (Ishizuka et al., 1990). The midline of the fimbria divides CA3 into the distal and proximal portions.

For statistical comparisons across more than two groups, we used the Kruskal-Wallis test (nonparametric one-way ANOVA) and the Mann-Whitney U test for group comparisons. Alpha levels ≤ 0.05 were considered significant. All the values were presented as mean $\pm$ SE.

Electrophysiology and LSPS

For electrophysiology and photostimulation mapping experiments, the slices did not go through the dye staining unless specified. To perform whole-cell recordings, cells were visualized at high magnification (60× objective) and patched with glass electrodes of 4–6 MΩ resistance that were filled with an internal solution containing (in mM) 126 K-gluconate, 4 KCl, 10 HEPES, 4 ATP-Mg, 0.3 GTP-Na, and 10 phosphocreatine (pH 7.2, 300–305 mOsm). The internal solution also contained 0.1% biocytin for cell labeling and morphological identification. The glass electrodes with the same resistance parameters as noted above were also used for extracellular field potential recording. Raw electrophysiological data were digitized at 10 kHz and stored on data-acquisition computers. Once stable whole-cell recordings had been achieved with good access resistance (usually <20 MΩ), the microscope objective was switched from 60× to 4× for laser scanning photostimulation (LSPS).

The LSPS method has been previously used in the neocortex and hippocampus (Brivanlou et al., 2004; Dantzker and Callaway, 2000; Shepherd et al., 2005; Weiler et al., 2008; Xu and Callaway, 2009). Under our experimental conditions, only neurons located within ~100 μm of the site of photostimulation fired action potentials. Therefore, laser photostimulation allowed high spatial-resolution activation of action potentials restricted to excitatory or inhibitory neurons close to the location of each photostimulation site. It also could be inferred that, under our LSPS mapping conditions and within our analysis window (see below), evoked synaptic currents reflect direct connections onto the recorded cell from the cells at or near the photostimulation sites in different hippocampal subfields. During mapping experiments, photostimulation was usually applied to 16 × 16 patterned sites (with an intersite space of 60–80 μm^2) covering the whole hippocampus in a nonraster, nonrandom sequence to avoid revisiting the vicinity of recently stimulated sites; whole-cell voltage-clamp recordings were made from the recorded neurons to measure photostimulation-evoked excitatory postsynaptic current (EPSC) responses at the holding potential between −60 and −65 mV, which was based on the empirically determined GABAergic reversal potentials at the developmental ages tested. After EPSC measurements, whenever it was possible, the recorded cells were also voltage-clamped at −10 to −20 mV to detect photostimulation-evoked inhibitory postsynaptic current (IPSC) responses. In separate experiments, the recorded neurons were held at +5 mV in voltage-clamp mode with cesium-containing internal solution to map IPSCs.

Photostimulation can induce two major forms of excitatory responses (Shi et al., 2010; Xu and Callaway, 2009), 1) direct glutamate uncaging responses (direct

activation of the recorded neuron's glutamate receptors) and 2) synaptically mediated responses (EPSCs) resulting from the suprathreshold activation of presynaptic excitatory neurons. Responses within the 7-msec window from laser onset are considered direct. Synaptic currents with such short latencies are not possible because they occur before the generation of action potentials in photostimulated neurons. To exclude direct responses, candidate EPSCs with their arrival times occurring within the direct response window (within 7 msec of the laser onset) are dismissed. Similarly, for inhibitory postsynaptic responses, we included only actual presynaptic inhibitory input (resulting from somatic firing of inhibitory neurons at stimulated locations) to construct inhibitory input maps. A technique that combines the design of a bank of approximately matched filters with the detection and estimation theory was implemented for automated detection and extraction of photostimulation-evoked EPSCs or IPSCs (Shi et al., 2010). As for individual map construction, input measurements from different stimulation sites were assigned to their corresponding anatomical locations in the hippocampus, and color-coded maps of average input amplitude, the number of events, and response latency per site were plotted to illustrate the overall input pattern to the recorded cell. The input amplitude/strength of each stimulation site was measured by the sum of individual EPSCs or IPSCs from each photostimulation site with the baseline spontaneous response subtracted and then normalized by the analysis window of 150 msec after photostimulation. This average integrated value was expressed in picoamperes (pA) for the analysis window. To compare input strength and connections across cell groups quantitatively, we measured the total sum of the ESPC or IPSC input strength across the map sites for individual cells and assessed the extent of synaptic connections by measuring the number of stimulation locations providing synaptic input in the mapping region. We also compared EPSC or IPSC latencies of data maps across the cell groups.

After all physiological assays had been completed, the brain slices were fixed in 4% paraformaldehyde in phosphate-buffered saline (PBS) overnight and then transferred to 30% sucrose solution in PBS. All the slices were stained for 4′-6-diamidino-2-phenylindole (DAPI; Sigma-Aldrich, St. Louis, MO) to identify hippocampal subfields. Those slices with whole-cell recording experiments were stained against biocytin with 1:1,000 Cy3-conjugated streptavidin (Jackson Immunoresearch, West Grove, PA), and cell morphology was examined with confocal or epifluorescence microscopy. Excitatory pyramidal neurons in CA3, hilar mossy cells, and DG granule cells were targeted for recordings based on their distinguishable morphology in living slices under differential interference contrast (DIC) microscopy and confirmed by post hoc analysis of their intrinsic spiking patterns and morphological features revealed by the biocytin staining.

RESULTS

Spontaneous GNA in the developing mouse hippocampus

We examined mouse hippocampal circuit activity in slice preparations at different ages (P1–P18) with VSD imaging, which monitors neuronal activity spanning DG and hippocampus simultaneously (Xu et al., 2010). We found that spontaneous GNA exhibits a specific anatomical origin at distal CA3, and it starts with sparse activation at the initiation site and gradually evolves into large-scale, bidirectional propagating network activity (Fig. 1; Supp. Info. Movie 1). GNA exhibits rather uniform patterns across different occurrences in the same slices. Simultaneous voltage-clamp recordings verified that individual cells receive excitatory synaptic input that correlates with optical measurement (Fig. 1A,B). GNA initiation is empirically determined by patches of coherent activation across five consecutive VSD image frames with its signal amplitude at least 1 SD above the preceding-50-msec baseline activity. As per the color scale, warmer colors indicate greater excitation. The initiation (first 20–30 msec) appears to arise from activation of a small number of neurons within the area of 80 μm × 80 μm (Fig. 1C,E; Supp. Info. Movie 1). GNA propagation starts after 40–50 msec and produces strong excitatory activity within 300–500 msec throughout the hippocampal circuitry, propagating to proximal CA3, then to the hilus and the fascia dentate of the DG as well as to CA1 (Fig. 1C,D). The propagation pattern of GNA could also be well illustrated in space–time analysis of the network activity (Fig. 1F,G); there is a U-shaped activity spread from the point of origin at distal CA3, indicating bidirectional propagation.

Mouse GNA appears robustly at P2, and event frequency peaks at P5–P6 (Fig. 2A). GNA event frequency of the first postnatal week is 0.66 ± 0.075 events per minute (N = 12 slices of P2–P7), which is considerably lower than an average of five or six events/minute for rat GDPs identified by intracellular recordings (Ben-Ari et al., 1989; Bolea et al., 1999), suggesting a potential species difference and a possibility that single-cell events may not correspond to global-scale events. GNA events occur significantly less often at later postnatal days (Fig. 2A), with an average rate of 0.36 ± 0.072 events per minute between P8 and P16 (N = 19 slices),
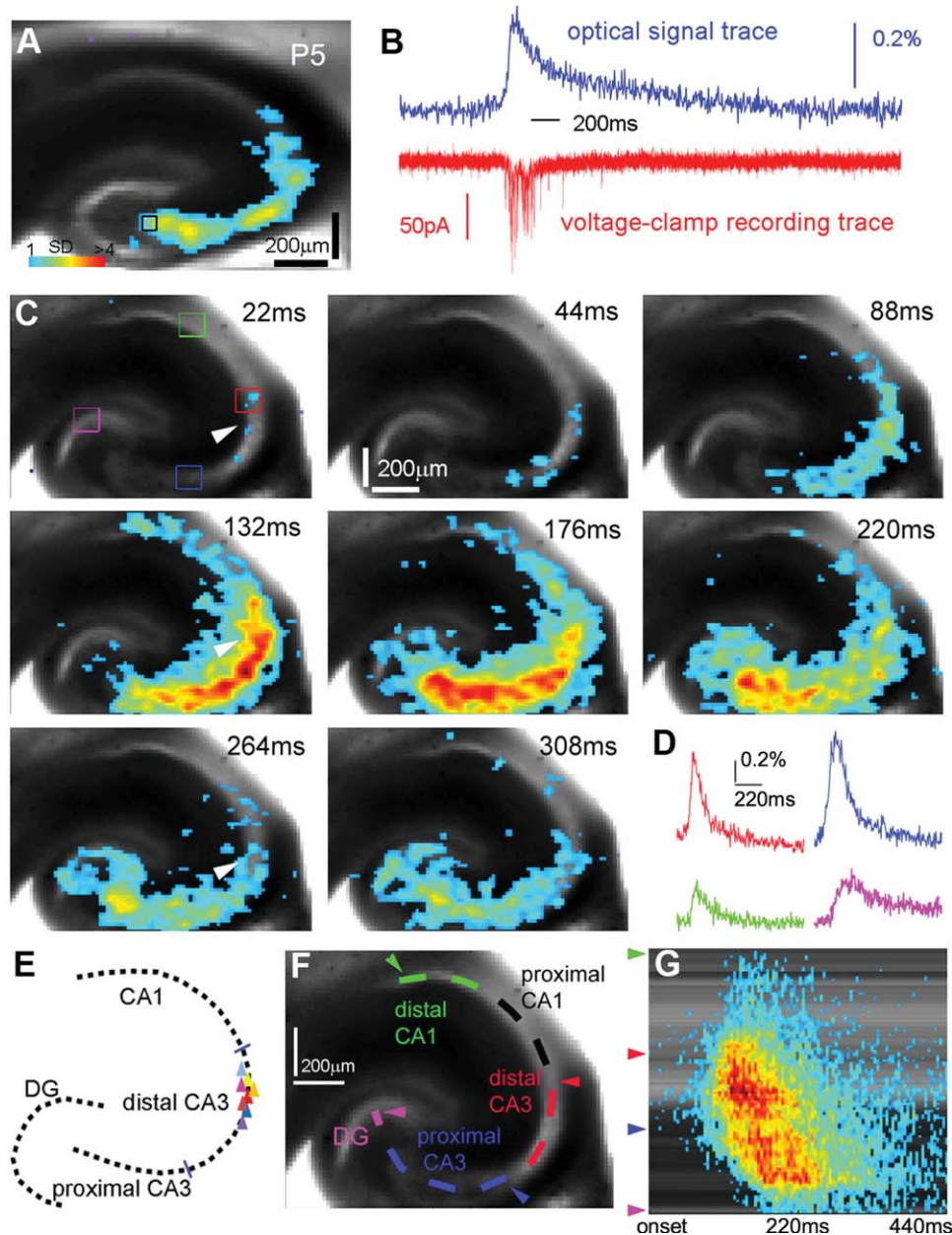
Figure 1. Spontaneous global network activation (GNA) in the developing mouse hippocampus exhibits both strong forward and backward propagation from distal CA3. **A,B:** Voltage-sensitive dye (VSD) imaging and simultaneous whole-cell recording indicate that GNA is tightly correlated with single neuronal activity. The measurements were taken from a proximal CA3 site as indicated by the small black square. The VSD image frame in A was plotted beginning at the peak of excitatory synaptic input to the recorded neuron. Color-coded activity is superimposed on the background slice image. The color scale codes VSD signal amplitude expressed as standard deviation (SD) multiples above the mean baseline. B shows the aligned optical signal trace (VSD signal in the percentage change of pixel intensity [$\Delta I/I\%$]) and voltage-clamp recording trace. **C:** Time series data from VSD imaging of spontaneous GNA. The arrowhead indicates the initiation site in distal CA3. **D:** Time courses of VSD signal from the regions of interest indicated by the colored rectangles in C are plotted from GNA onset. **E:** Schematic distribution of spontaneous GNA initiation zones (eight representative slices). Each triangle represents one slice sample. **F,G:** Space–time analysis of GNA propagation shown in B. F shows an analysis curve aligned with the hippocampal circuitry in the slice image, and G is the space–time map with the y-axis indicating the location along the analysis curve shown in F (e.g., the green, red, blue and pink arrowheads correspond to those sites indicated in F) and with the x-axis denoting the time progression from the activity onset.

which differs significantly from P2 to P7 ($P < 0.01$). GNA is detected in only 40%, and 20% of the more developmentally mature slices tested at P10–P12 and P13–P16, respectively, compared with 80% of the slices for P2–P9. No GNA events are detected beyond P18. Overall, there was no discernible trend for clustered
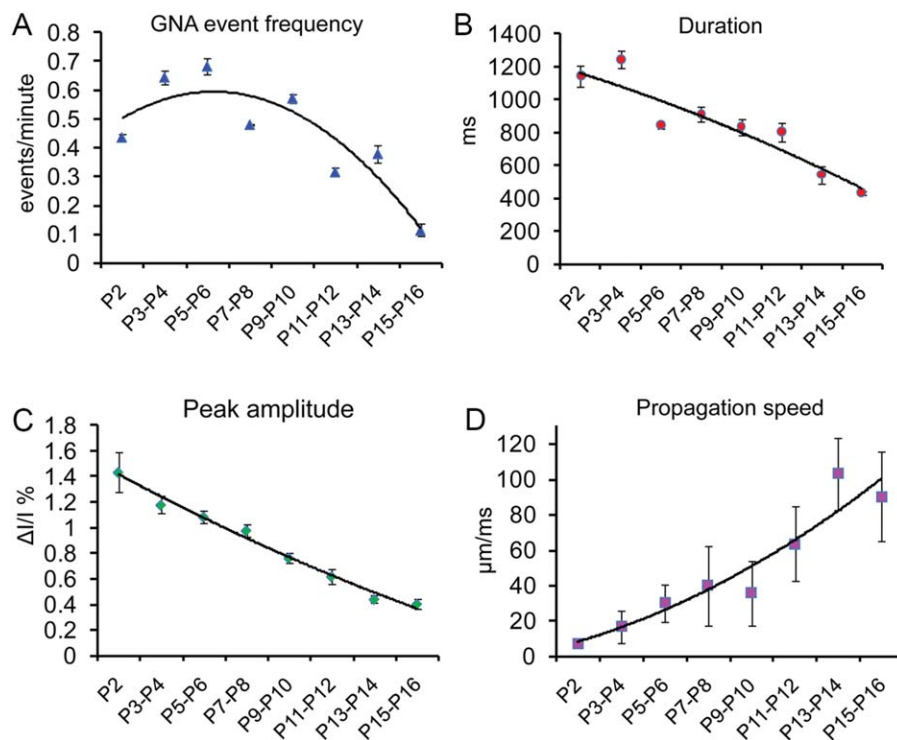
Figure 2. Developmental changes of GNA. **A–D:** Average GNA event frequency, duration, peak amplitude, and propagation speed, respectively, during P2–P16. The curves are polynomial fits through data points (each measured from several sampled events from four or five slices). The values represent mean ± SE.

occurrences by trial as we examined a scatterplot of GNA occurrences vs. trial numbers from selected sessions in P3–P8 slices (N = 88 sessions from eight slices). The average numbers of events per session for a given slice was 0.92 ± 0.10, with its intersession SD of GNA occurrence ranging from 0.7 to 1.2.

In addition, GNA event duration decreases with increasing age from P2 onward (Fig. 2B), the average durations of P2–P7 and P9–P16 being 1,083.7 ± 76.9 msec and 719.8 ± 49.1 msec ($P < 0.005$), respectively. Each GNA occurrence appears to last longer than intracellularly recorded rat GDPs (400–800 msec; Ben-Ari et al., 1989; Bolea et al., 1999) and extracellularly detected spontaneous field potential fluctuations, SPWs (50–100 msec; Buhl and Buzsaki, 2005; Maier et al., 2003). Moreover, the GNA amplitude decreases with increasing postnatal age (Fig. 2C); the average peak amplitudes across slices were 1.17% ± 0.19%, measured with the percentage change in pixel light intensity (ΔI/I%), and 0.56% ± 0.17% for P2–P7 and P9–P16 slices ($P < 0.001$), respectively (Fig. 2C). However, the velocity of activity propagation as measured by the travelling peak of VSD signal (Fig. 1G) increases with age, going from 8.8 ± 3.2 μm/msec during P2–P4 to 28.6 ± 10.6 μm/msec during P5–P7 and to

90.1 ± 25.6 ($P < 0.01$) μm/msec during P9–P16 (Fig. 2D). Overall, mouse GNA exhibits developmental changes, which likely is related to circuit maturation. The adult-like pattern of unidirectional circuit propagation from DG to CA3 to CA1 appears at about 2 weeks of age (see below), so the later time points for GNA duration, peak amplitude and propagation speed may reflect fundamentally different underlying processes at earlier (P2) vs. later (P15–16) times.

Interestingly, mouse GNA in the first postnatal week is different from GDPs reported in the rat based on differences between their pharmacological properties. GNA is not suppressed by blocking GABAergic transmission via $GABA_A$ receptor antagonists (gabazine, SR95531, or bicuculline). Although GNA frequency, amplitude, and propagation speed at P2–P5 do not change significantly in the presence of gabazine (Fig. 3A,B), GNA at P7–P10 is enhanced by gabazine (Fig. 3D,E; N = 5–6 slices each). The changes of GNA properties in the presence of gabazine at P2–P5 vs. P7–P10 were quantified and are summarized in Figure 4. In contrast, mouse GNA is completely abolished by the AMPA receptor antagonist 6-cyano-7-nitroquinoxaline-2,3-dione (CNQX; N = 10 slices). Furthermore, the NMDA receptor antagonist 3-(2-carboxypiperazin-4-yl)propyl-1-
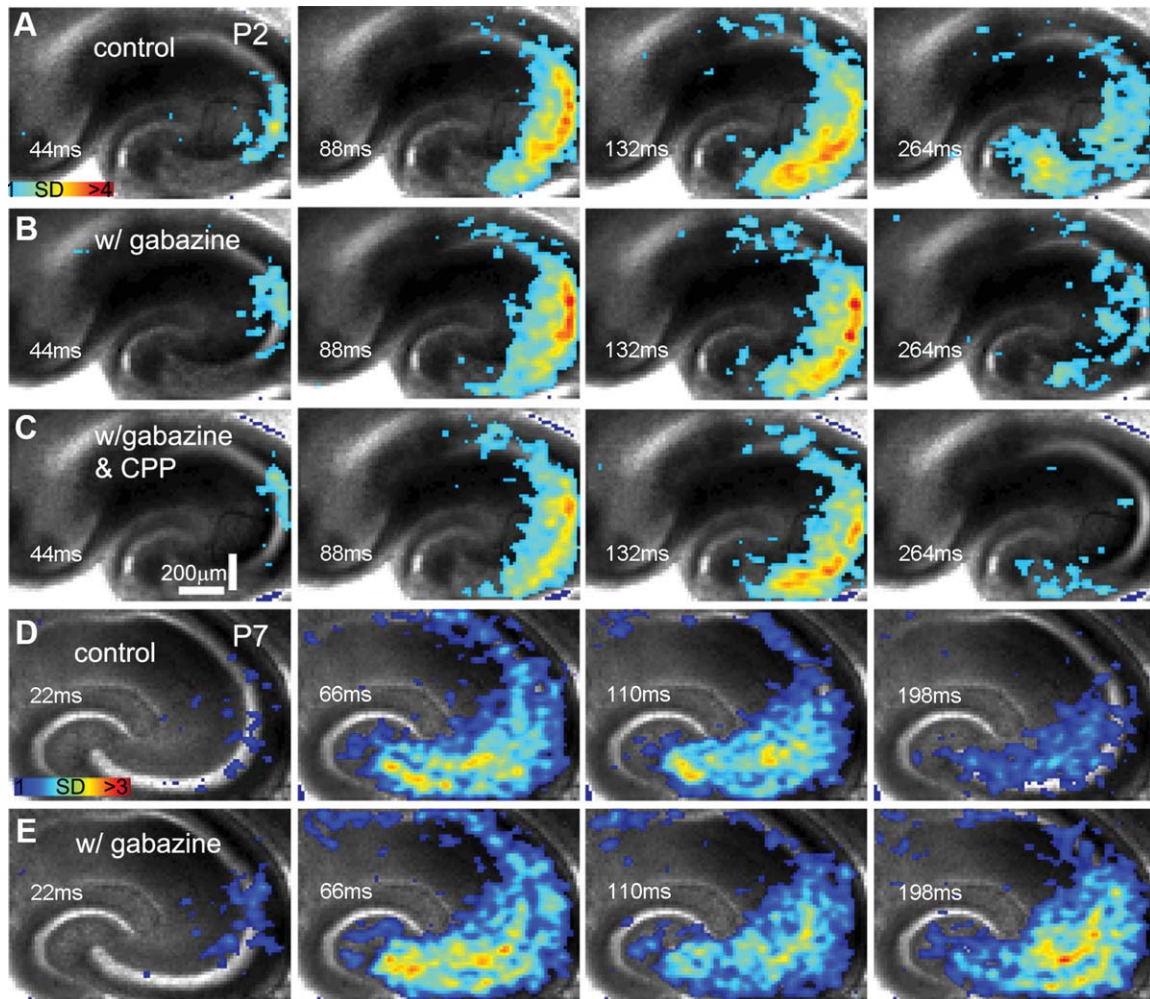
Figure 3. The initiation and propagation of spontaneous GNA does not require GABA$_A$ receptor- or NMDA receptor-mediated signal transmission. A–C and D,E show time series data from the P2 and P7 slices, respectively. **A–C:** Spontaneous GNA in normal recording solution, in the presence of the GABA$_A$ receptor antagonist gabazine (20 μM) and in the presence of gabazine and the NMDA receptor antagonist CPP (10 μM), respectively. The color scale corresponds to VSD signal amplitude expressed as SD multiples above the mean baseline. **D,E:** Spontaneous GNA in normal recording solution and in the presence of gabazine (20 μM), respectively.

phosphonic acid (CPP), with or without gabazine, does not block the onset or propagation of this network activity (Fig. 3C). Thus, the initiation and propagation of spontaneous GNA identified in the mouse hippocampus is controlled by glutamatergic transmission mediated by AMPA receptors rather than GABA$_A$ or NMDA receptors.

Correlation among single-cell events, field potential recordings, and GNA

To address the cellular basis of mouse GNA, we first examined spontaneous activity of excitatory pyramidal neurons in CA3 of P5–P6 mouse hippocampus. As shown in Figure 5A,B, our data indicate that spontaneously recurring, long-duration membrane potential depolarizations of single neurons may underlie GNA macroscopically detected by VSD imaging. Most neurons recorded

are spontaneously active, displaying large and persistent depolarizations of 20–50 mV superimposed with bursts of spikes that are electrophysiologically similar to rat GDPs. The average frequency of these persistent depolarizations sampled from six excitatory neurons (P5–P6) was 1.48 ± 0.30 events/minutes, and their average duration was 1.29 ± 0.09 seconds. Gabazine does not abolish persistent depolarizations but reduces their overriding spiking activity, which makes large membrane depolarizations more prominent. All spontaneous spiking activity and depolarizations are blocked by CNQX. Overall, these properties of long-duration cellular depolarizations (electrophysiological equivalent of GDPs in mouse hippocampus, mouse GDPs) are consistent with GNA properties.

Because a developmental shift of GABA effects from mixed inhibition and excitation to exclusive inhibition
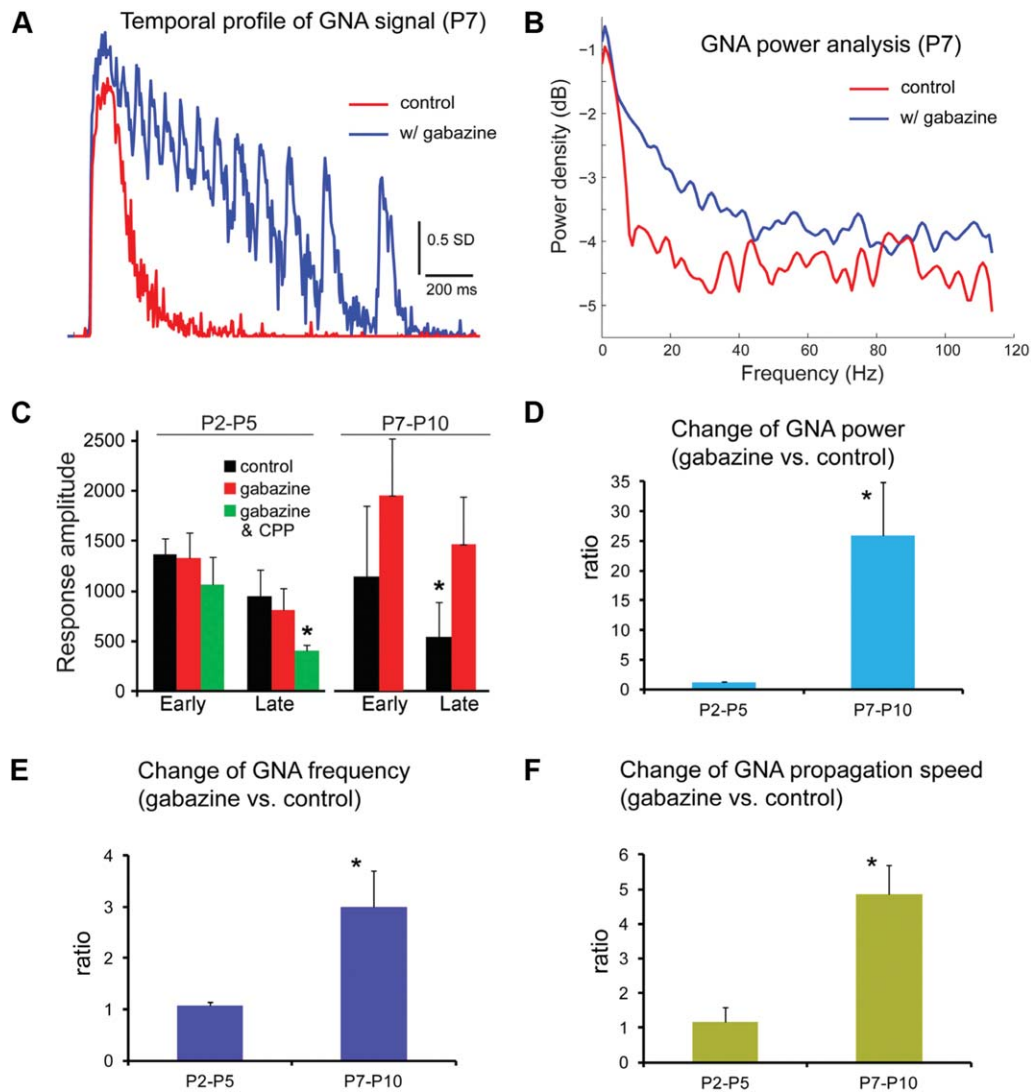
Figure 4. Characterization of changes of GNA properties in the presence of gabazine in comparison with the control condition. **A:** Temporal profiles of GNA from the CA3 region of the P7 slice illustrated in Figure 3D,E for control and gabazine conditions, respectively. **B:** Power density function analysis of GNA for control and gabazine conditions of the P7 slice, which clearly shows increased power at higher oscillation frequencies. **C:** Average response amplitude (early and late response phases) of GNA across the entire hippocampus at P2–P5 and P7–P10 (N = 5–6 slices each) with different experimental conditions. The early and late response phases are defined as the time durations of 66–132 msec and 198–264 msec postphotostimulation, respectively. The summed response amplitude of activated pixels is in units of SD. $*P < 0.05$ compared with control. The bar graphs represent mean $\pm$ SE. **D–F:** Changes of GNA power, frequency, and propagation speed in the presence of gabazine, respectively. For the GNA power analysis, the VSD signal was acquired by averaging the pixels across the CA3 region from each image frame; the averaged values constituted the data points of the VSD signal trace in temporal order. The signal trace was detrended by linear regression to remove the baseline drift and then subtracted by its mean. The "pwelch" function in Matlab was used to calculate the power values at different frequencies, which were summed to obtain the GNA power for the signal trace. In D, the power ratios of P2–P5 and P7–P10 GNA events (N = 9–12 each) are 1.17 ± 0.19 and 25.9 ± 9.0, respectively. In E, the frequency ratios of P2–P5 and P7–P10 slices are 1.06 ± 0.07 and 3.0 ± 0.7, respectively. In F, the speed ratios of P2–P5 and P7–P10 events are 1.16 ± 0.42 and 4.86 ± 0.83, respectively. The y-axis indicates the average ratio of the parameter measured in the presence of gabazine compared with the control condition. $*P < 0.05$ compared with control.

occurs between P6 and P10, we further tested the effects of blocking GABA$_A$ receptor-mediated activity at P10, the older age. To examine the effects of gabazine on single-cell events at an older age, we recorded from CA3 pyramidal cells (N = 5 cells) in P10 mouse hippocampus.

In control ACSF, the average frequency of mouse equivalent GDPs sampled from the P10 excitatory neurons was 0.33 ± 0.13 events/minute, and their average duration was 0.67 ± 0.11 seconds. We found that gabazine led to enhanced circuit excitation with more frequent and large
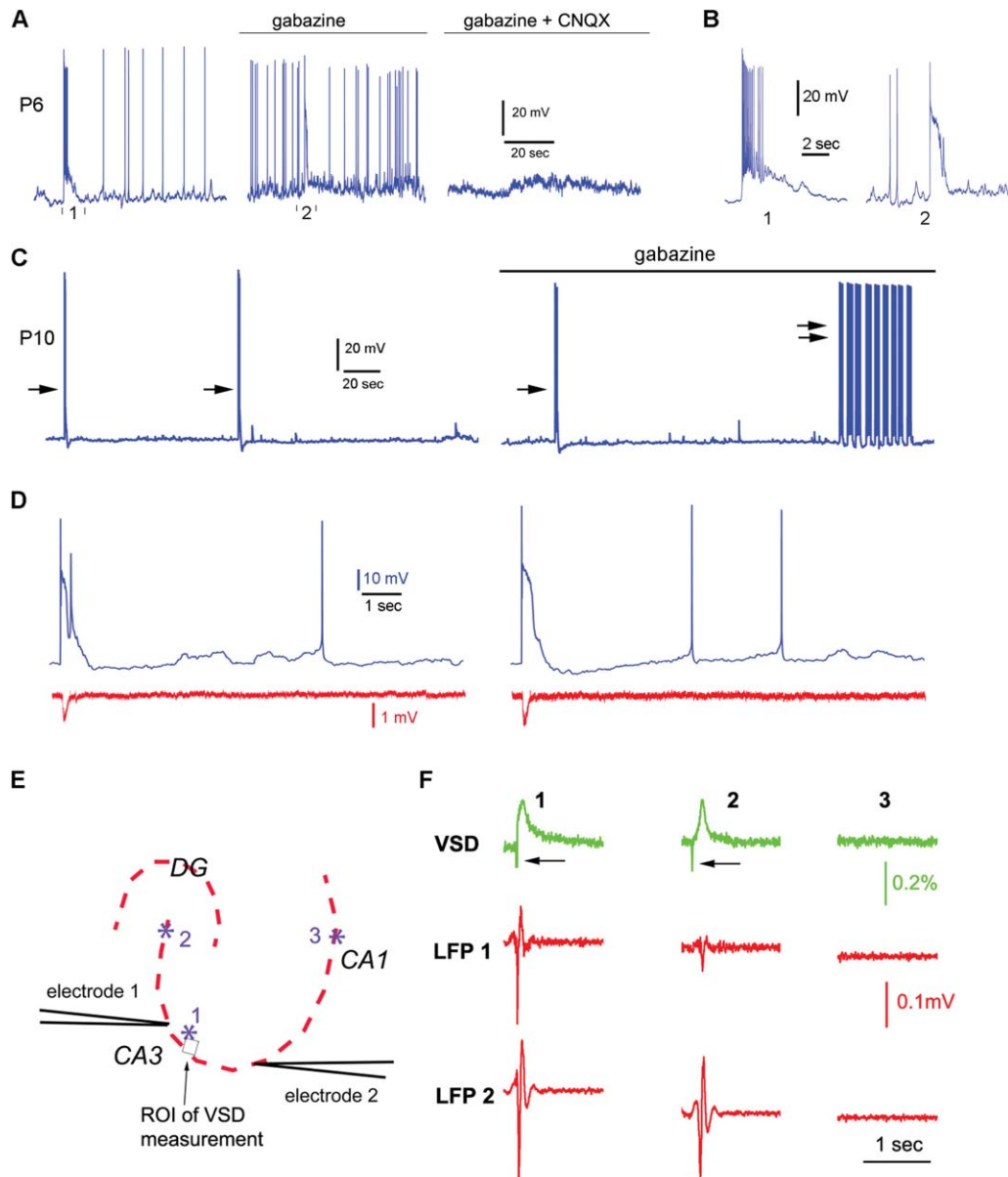
Figure 5. Correlation among single-cell events, field potential recordings, and GNA. **A:** Spontaneous activity of an example CA3 excitatory neuron (P6) in normal recording solution, in the presence of gabazine, and in the presence of both gabazine and CNQX (left, middle, and right, respectively). **B:** The long-duration depolarization indicated by "1" and "2" in A, expanded and shown separately. **C:** Spontaneous activity of a CA3 excitatory neuron (P10) in normal recording solution and in the presence of gabazine (left and right, respectively). Single arrows point to typical long-duration depolarizations, and double arrows point to "epileptiform" activity. **D:** Examples of the occurrence of long-duration cellular depolarization (but not the spontaneous recurring narrow spikes) coinciding with the occurrence of local field potential (LFP) events in P5–P6 slices. The membrane potential trace and the LFP signal trace are shown in blue and red, respectively. **E,F:** GNA occurrences detected by two-site field recordings in CA3 in P5–P6 slices. E shows the LFP electrode placement and photostimulation sites (1, 2, 3) in the imaged slice. F shows simultaneous VSD and LFP detection in response to photostimulation of the sites (1–3) in E. The VSD signal was measured from the small region of interest (ROI) close to the site 1. The occurrences and propagation of GNA in response to photostimulation at the sites of 1 and 2 are reflected by the detection of LFP events from the two electrodes, whereas the local response in CA1 (site 3) did not induce GNA or lead to the LFP detection in CA3. The LFP signal traces were bandpass filtered at 5–300 Hz.

subthreshold EPSPs (Fig. 5C), which is consistent with GABA action at this older age. Although typical mouse GDPs (single arrows in Fig. 5C) seen in control ACSF solution continued to occur in the presence of gabazine, at P10 gabazine promoted excitation resembling epileptiform activity (double arrows in Fig. 5C).

We also examined the relationship between mouse GDPs and local network events as detected by field
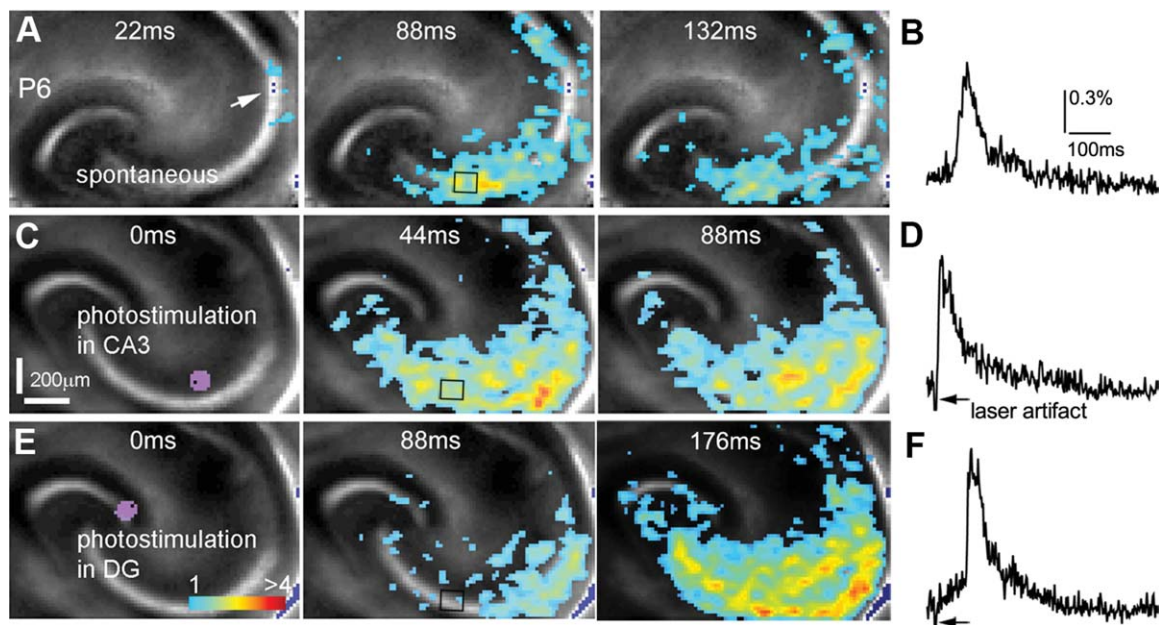
Figure 6. Photostimulation-evoked GNA mimics spontaneous GNA in spatiotemporal patterns. **A:** Time series data of imaging spontaneous GNA at P6. The arrowhead points to the initiation site in distal CA3. **B:** The time course of VSD signal (in the percentage change of pixel intensity [$\Delta I/I\%$]) from the region of interest indicated by the small rectangle in the second image frame in A. **C:** Time series data of imaging evoked GNA after spatially restricted laser photostimulation (via glutamate uncaging) in distal CA3. The site of photostimulation can be identified by the laser excitation artifact (purple) in the first frame. **D:** Time course of VSD signal from the region of interest indicated by the small rectangle in the second image frame in C. **E:** Time series data of imaging evoked network activity after spatially restricted laser photostimulation in DG. **F:** The time course of VSD signal from the region of interest indicated by the small rectangle in the second image frame in E. Note that A, C, and E are images from the same slice, but C and E were acquired by the camera with an angle of rotation.

recording with the electrode placed in the pyramidal cell layer at 100–200 μm away from the single cells examined (N = 8 P5–P6 cells; Fig. 5D). During the experiments, photostimulation using caged glutamate (see below) was delivered at a few sites around the recorded cells to induce the occurrence of mouse GDPs. We found that a great majority (86.6%) of the occurrences of long-duration cellular depolarization coincide with tight onset with the detection of local field potential (LFP) events (82 single cell events/71 field recording events), the LFP duration being 51.8% of that of long-duration cellular depolarization, as would be expected from extracellular averaging of intracellular events. This indicates that most mouse GDPs closely relate to LFP events reflecting neuronal ensemble behavior in local circuits.

In addition, we examined the correlation between GNA and LFP events by comparing photostimulation evoked GNA and locally detected field events (Fig. 5E,F). Every GNA occurrence is detected by two-site LFP recording separated at 200–300 μm apart in CA3 (N = 61 events from 7 P5–P6 slices), and the stronger VSD signal correlates with the stronger field potential response. The LFP response was faster than the VSD

signal; its peak of downward response (excitatory field response in the pyramidal cell layer [Lamsa et al., 2000]) occurs 25.7 ± 2.6 msec ahead of the VSD signal peak, bcause of different kinetics of the electrical vs. the dye signal. Thus, at least in these particular experiments, local field events are tightly correlated with GNA, which indicates that LFP and GNA may measure the same underlying phenomena at different scales.

Photostimulation-evoked population activity in the developing mouse hippocampal circuitry

To examine further the developing hippocampal circuit activity in the first postnatal week, we used laser photostimulation via glutamate or GABA uncaging to evoke population neuronal activity in defined sites of spontaneous GNA origin. Caged compounds that are rendered biologically inert by the chemical addition of a light-sensitive "caging" group were infused into the slices. Upon illumination with UV laser, biologically active glutamate or GABA is liberated from the cage group and binds to its cellular receptors. The laser beam forms uncaging spots, each approximating a Gaussian
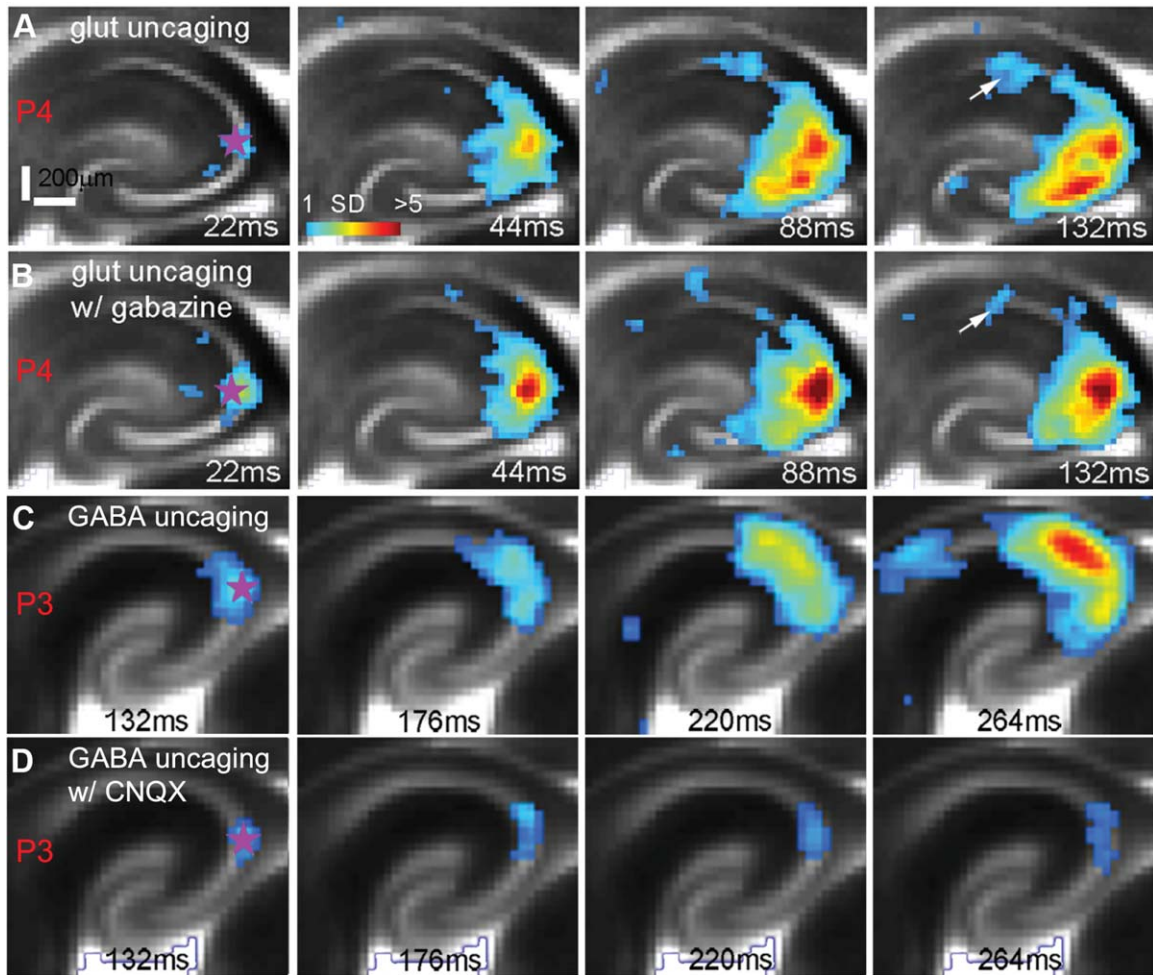
Figure 7. Mouse GNA is dominated by AMPA receptor-mediated glutamatergic transmission. **A,B:** Photostimulation-evoked network activity by glutamate uncaging in a P4 slice was largely unaffected by the GABA$_A$ receptor antagonist gabazine (20 µM). The uncaging site is denoted by a purple star. The arrows indicate some reduced propagation to CA1 in the presence of gabazine. **C,D:** The propagation of photostimulation-evoked network activity by GABA uncaging in a P3 slice was abolished by the AMPA receptor antagonist CNQX (10 µM). The excitatory response at the uncaging site in D was blocked by the further application of gabazine with CNQX. Note that photostimulation and imaging of both slices were performed through a 2× objective.

profile with a width of ~100 µm laterally at the 4× objective focal plane (Fig. 6; see also Xu et al., 2010).

Spatially restricted glutamate uncaging in mouse distal CA3 (Fig. 6C,D) was found to evoke population neuronal activity with features similar to those of spontaneous GNA (Fig. 6A,B), with excitatory activity beginning at the site of photostimulation and propagating bidirectionally, toward proximal CA3 and DG as well as toward CA1. The evoked activity has an average latency of 15.5 ± 3.9 msec and an average duration of 746.3 ± 60.9 msec, with an average peak amplitude of $1.68\% \pm 0.22\%$ (N = 13 slices). Similar to spontaneous GNA, the propagation speed of evoked activity increases later in development, increasing significantly ($P < 0.005$) from 6.5 ± 0.7 µm/msec in P2–P4 to 22 ± 5.5 µm/msec in P5–P7. Additionally, during P2–

P5, gabazine does not appear to affect evoked network activity significantly (Fig. 7A,B) but enhances excitatory activity evoked by glutamate uncaging in the second postnatal week (N = 7 slices), matching the behavior of spontaneous GNA. In addition to distal CA3, other parts of the hippocampal circuitry were photostimulated. In the first postnatal week, evoked activity in DG propagates to CA3 and then spreads from CA3 to CA1 along the trisynaptic circuitry in the early phase, but there is clear back-propagation from CA3 to DG in the late response phase (Fig. 6E,F), which mimics the activity induced by distal CA3 photostimulation and spontaneous GNA. However, photostimulation in CA1 does not lead to backward propagation to CA3. Therefore, backward or reverse propagation in the developing circuitry indicates a strong excitatory pathway from CA3 to the
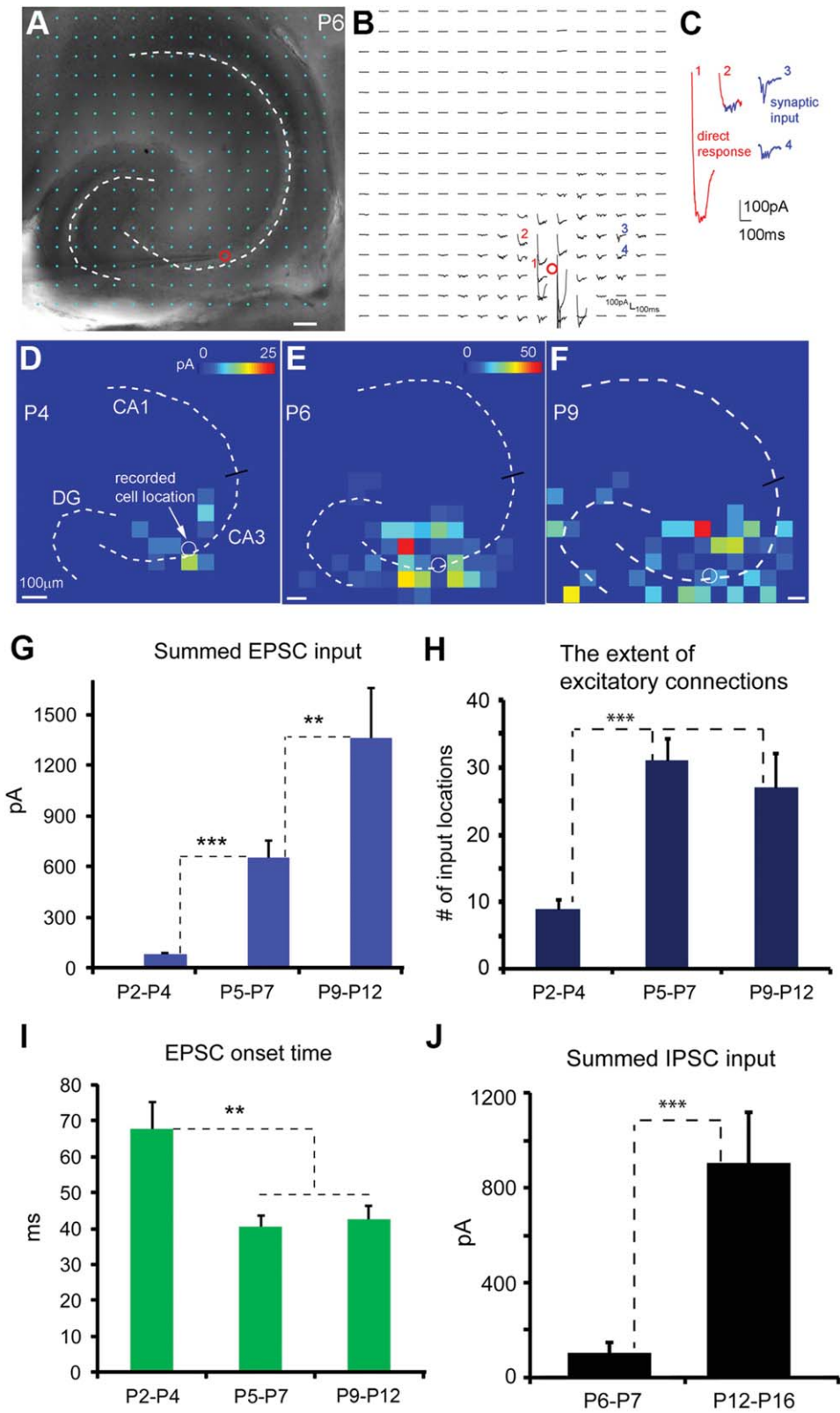
Figure 8.

hilus and the fascia dentate of DG, which does not appear in mature circuitry (Scharfman, 1994, 2007).

We also examined the circuit response to GABA uncaging (N = 14 slices). Localized excitatory responses are observed at the uncaging sites in mouse slices from P1 to P5, whereas excitatory activity is no longer clear at P6–P7. In the younger slices, sometimes GABA uncaging in CA3 induces propagating network activity (N = 5 slices) similar to glutamate uncaging (Fig. 7C), although GABA uncaging has a longer response latency (85 ± 13 msec). GABA-evoked propagating activity is blocked by the AMPA receptor antagonist CNQX, leaving only a localized response at the GABA uncaging site (Fig. 7D). This indicates that GABA can excite neonatal neurons and contribute to the initiation of spontaneous activity, but the propagation of excitatory activity in the developing mouse hippocampal circuitry is determined by AMPA receptor-mediated transmission.

GNA and circuit connections

To establish the temporal relationship between GNA and the maturation of functional circuit connections, we mapped the development of hippocampal neural circuitry over the time during which GNA is active. First, synaptic connections to excitatory pyramidal neurons were mapped by combining whole-cell recordings with LSPS (Ikrar et al., 2011; Shi et al., 2010). As illustrated in Figure 8A–C, the LSPS approach involves first recording from a single neuron, then stimulating at other sites in order to generate action potentials from neurons in those sites; recording from the potential postsynaptic neuron allows one to determine whether there is actual synaptic input from one particular site. By sequentially stimulating many different sites across the hippocampus, it is possible to generate a map of locations of neurons providing input to that one cell. Through the LSPS mapping experiments, we found that there is

clearly observable strengthening of excitatory and inhibitory connections to CA3 pyramidal neurons over the developmental time course (Fig. 8D–J). Younger neurons (e.g., P2–P4) have weaker synaptic connections with more localized input from around the perisomatic region, whereas older neurons (e.g., P9–P12) have stronger and more extensive synaptic connections from a wider area (Fig. 8D–F). DG connections to CA3 neurons are increasingly strengthened at older ages, as illustrated in the example maps. The average, summed excitatory synaptic input strengths measured from excitatory pyramidal cells are 80.8 ± 10 pA (N = 10 cells), 650.4 ± 99.9 pA (12 cells), and $1,362.7 \pm 292.9$ pA (8 cells) for the three age groups (P2–P4, P5–P7, P9–P12), respectively (Fig. 8G). The extent of local excitatory connections also increases significantly from P2–P4 to P5–P12 by measuring the numbers of input-mapped locations (Fig. 8H). Along with the enhanced input strength, synaptic responses at P5–P7 and P9–P12 have overall shorter latencies than P2–P4 (median latencies 67.6 ± 7.6 msec, 40.6 ± 2.9 msec, and 42.7 ± 3.5 msec for P2–P4, P5–P7, and P9–P12, respectively; Fig. 8I). In addition, inhibitory synaptic connections to pyramidal cells can be detected by measuring inhibitory postsynaptic currents (IPSCs) to the recorded neurons at the end of the first postnatal week and are clearly enhanced during the second week. The average, summed inhibitory synaptic input strengths measured from excitatory pyramidal cells are 104 ± 41.5 pA (N = 6 cells) and 904.1 ± 215 pA (11 cells) for the age groups P6–P7 and P12–P16, respectively.

We also correlated functional circuit connectivity with cell morphological development by examining the overall dendritic morphology of CA3 excitatory pyramidal cells as revealed by intracellular biocytin labeling in early developing hippocampus. There is a rapid

Figure 8. Developmental strengthening of local synaptic connections to CA3 excitatory pyramidal neurons. **A–C:** Laser scanning photostimulation combined with whole-cell recordings to map circuit connections to single neurons. A: Mouse hippocampal P6 slice image with the superimposed photostimulation sites (16 × 16 cyan, spaced at 80 μm × 80 μm). B: Photostimulation-evoked response traces from the corresponding sites in A, with the recorded cell held in voltage-clamp mode to detect inward excitatory postsynaptic currents (EPSCs). The red circle indicates the recorded cell body location. Different forms of photostimulation responses are illustrated by the traces, which are expanded and shown separately in C. Trace 1 is an example of a large direct response (excluded for further analysis) to glutamate uncaging on the cell body. Trace 2 shows an example of relatively small direct response, with overriding synaptic responses (blue). Traces 3 and 4 are typical examples of synaptic input responses. **D–F:** Color-coded synaptic input maps showing local excitatory connections to representative CA3 cells at P4, P6, and P9, respectively. The input maps are constructed based on quantification of photostimulation-evoked excitatory synaptic input at stimulation sites across the hippocampus (see Materials and Methods). The color scale codes average input strength at each stimulation site. The amplitude scale in E applies to E and F. The spatial scale in A or D-F is 100 μm. **G–I:** Quantitative comparison of synaptic input strength, the extent of excitatory connections, and the response latencies across CA3 excitatory neurons of P2-P4 (N = 10 cells), P5-P7 (N = 12 cells), and P9-P12 (N = 8 cells). Specifically, G-I show the measurements of the average summed EPSC input strength to single CA3 cells, the average number of input locations, and the average onset times of the first detected EPSC per site, respectively. **J:** Quantitative comparison of inhibitory synaptic input strength to CA3 excitatory neurons for the age groups P6-P7 and P12-P16 (N = 6 and 11 cells, respectively). **P < 0.01, ***P < 0.001 between groups.
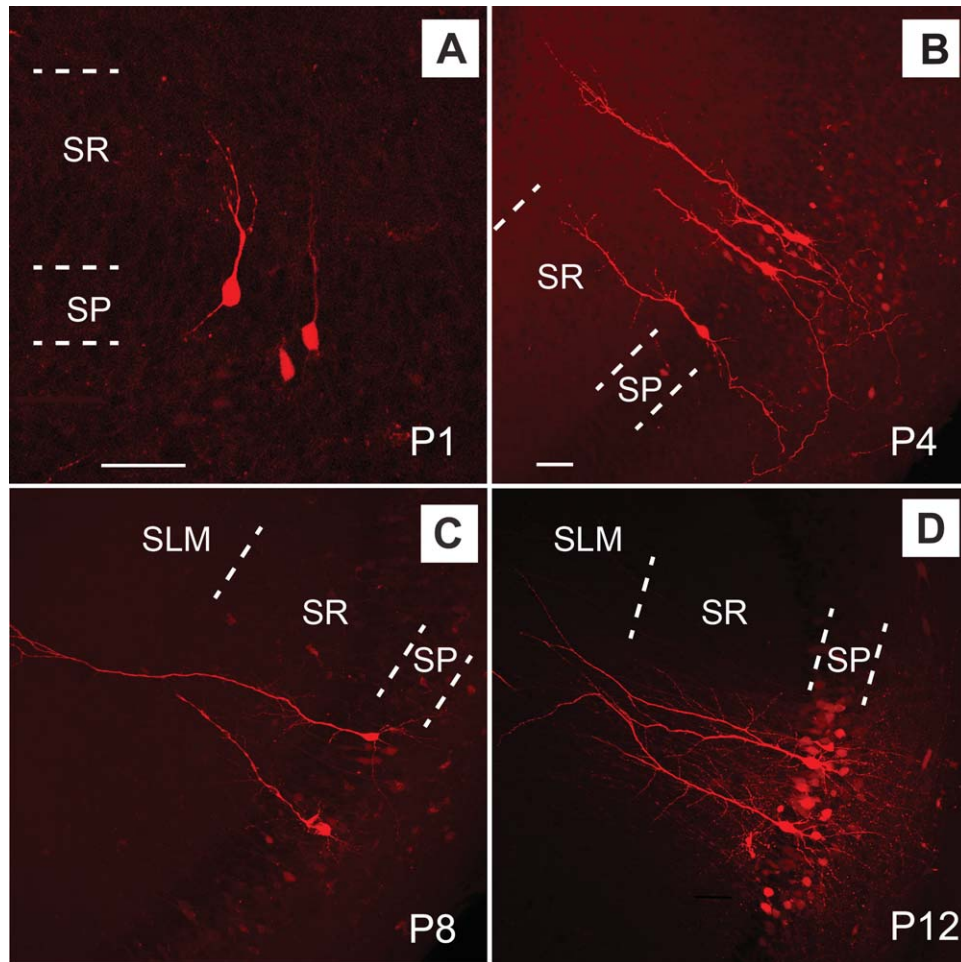
Figure 9. Morphology of CA3 excitatory pyramidal cells in the developing mouse hippocampus. **A–D:** Gross morphology of example pyramidal cells of P1, P4, P8, and P12, respectively, revealed by intracellular biocytin labeling. Compared with older ages, P1–P4 cells have much shorter apical dendrites. SP, stratum pyramidale; SR, stratum lucidum and radiatum; SLM, stratum lacunosum moleculare. Scale bars = 50 μm in A; 50 μm in B (applies to B–D).

dendritic expansion of CA3 pyramidal cells during the first 2 postnatal weeks (Fig. 9). Consistent with their wider input connections revealed by photostimulation mapping, compared with P1–P4 (Fig. 9A,B), CA3 excitatory pyramidal cells have much wider dendritic fields and more extensive branches at or beyond P7 (Fig. 9C,D). The average apical dendritic lengths for selected P1–P4 cells and P7–P8 cells were 79.1 ± 12.2 μm, and 521 ± 15 μm, respectively ($P < 0.01$; N = 5 cells each).

To examine the underlying pathways accounting for GNA back-propagation from CA3 to DG, we further examined the circuit connections to excitatory mossy cells in the hilus and DG granule cells. For the mouse developing hippocampal slices (P4–P6), we found that mossy cells receive strong excitatory input from proximal CA3 (average strength 228.9 ± 58.9 pA measured from N = 8 cells; Fig. 10A). Although DG granule cells have much weaker local input compared with hilar

mossy cells, they receive excitatory input from the hilus and proximal CA3 (average strength 14.6 ± 3.8 pA and 12.1 ± 3.5 pA, respectively, measured from N = 7 cells; Fig. 10B). Therefore, GNA back-propagation from CA3 to DG likely is mediated through the disynaptic circuit of proximal CA3 pyramidal cells→hilar mossy cells→DG granule cells or the monosynaptic circuit of proximal CA3 pyramidal cells→DG granule cells.

In conjunction with the circuit mapping of single cells, photostimulation and VSD imaging were used to measure evoked circuit excitability and the directionality of excitatory signal propagation over P2–P15. In examining the photostimulation-evoked VSD response at two different uncaging sites (DG vs. distal CA3) across developmental times, it is obvious that younger slices are more excitable than older slices at both sites with more extensive and stronger response propagation (Fig. 11A–D). The VSD response strengths at glutamate
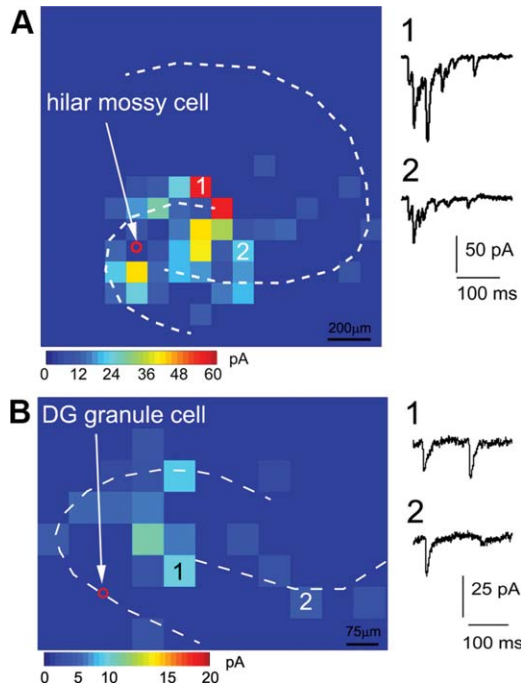
Figure 10. Local excitatory synaptic connections to hilar mossy cells and DG granule cells reflect the underlying pathways of the GNA back-propagation from CA3 to DG. **A,B:** Example excitatory input maps to one hilar mossy cell and a DG granule cell (P4–P6), respectively. As shown in A, mossy cells, the only excitatory cells in the dentate hilus, receive robust excitatory input from proximal CA3 area in addition to DG and the hilus. As illustrated in B, the granule cells receive relatively strong excitatory input from the hilus and weaker input from DG and proximal CA3.

uncaging sites are 1.46% ± 0.09% (P2–P7, N = 10 slices) and 0.48% ± 0.04% (P9–P15, N = 12 slices) for younger and older slices, respectively. Backward propagation from distal CA3 to DG in the first postnatal week is robust (Fig. 11B). However, although DG signaling to CA3 is maintained (Fig. 11C), the back-propagation to DG from distal CA3 is significantly decreased toward the end of the second postnatal week (Fig. 11D). This is supported by the finding that DG activation at P11–P14 (N = 6 slices) was much less than that at P7–P10 (N = 5) in response to distal CA3 photostimulation. Therefore, the emergence of the canonical unidirectional trisynaptic circuit organization in the developing hippocampus concurs with the disappearance of spontaneous GNA at about P14–P16.

DISCUSSION

Spontaneous network activity early in development is considered an important factor for sculpting and refining developing circuit architecture. Our approach to studying the developmental contributions of spontane-

ous and correlated neuronal activity in hippocampus is to determine which events are closely linked to establishing adult functional circuit organization. In this work, we identified and characterized a global pattern of activity that we term *spontaneous GNA* and a major transition of functional circuit organization in the developing mouse hippocampus from large-scale bidirectional signal propagation to the adult-like form of the canonical unidirectional trisynaptic circuit.

Terminology and technical considerations

We coined *spontaneous GNA* as a new term to describe spontaneous network events in developing mouse hippocampus, based on large-scale VSD imaging of global circuit events. In the same way, the terms *SPWs* and *GDPs* were coined to refer specifically to the events at single-cell and localized-circuit levels; we use GNAs to describe large-scale spontaneous network events in developing mouse hippocampus measured by macroscopic VSD imaging. Although there are some similarities between spontaneous GNA and the previously examined localized activity patterns, there are differences that indicate that spontaneous GNA does not correspond directly to such local events as GDPs or SPWs recorded with other techniques from the rat (Ben-Ari et al., 1989, 2007; Buhl and Buzsaki, 2005; Buzsaki, 1986; Leinekugel et al., 2002). Whereas rats GDPs depend on GABAergic transmission (Ben-Ari et al., 2007), mouse GNA is not abolished by GABA$_A$ receptor antagonists. We also observed an obligatory contribution of glutamatergic signaling through AMPA receptors required for mouse GNA. Single-cell GDP-like events are likely components of the summed macroscopic-circuit events that we measure as mouse GNA, but they can be distinguished by differing pharmacological sensitivities between the species. In addition, aside from scale, GNA captures emergent properties not described for GDPs, notably, the bidirectionality of signal propagation from distal CA3 origin to both CA1 and dentate gyrus. In a previous study using fast VSD imaging, Bolea et al. (2006) referred to GDP-related network events as neuronal coactivation in the developing rat hippocampus, in which a propagating excitation wave could be initiated from a small site and propagate to larger hippocampal circuitry. In contrast to what we observed for mouse GNA, the authors reported that GDP-related waves can originate both in the hilus and in CA3 and that the initiation site is not fixed and varies from event to event.

Although the question of whether GNA, GDPs, and SPWs are different facets of the spontaneous activity patterns in hippocampus remains to be further addressed, we have significantly built on earlier findings on spontaneous network activity in the developing
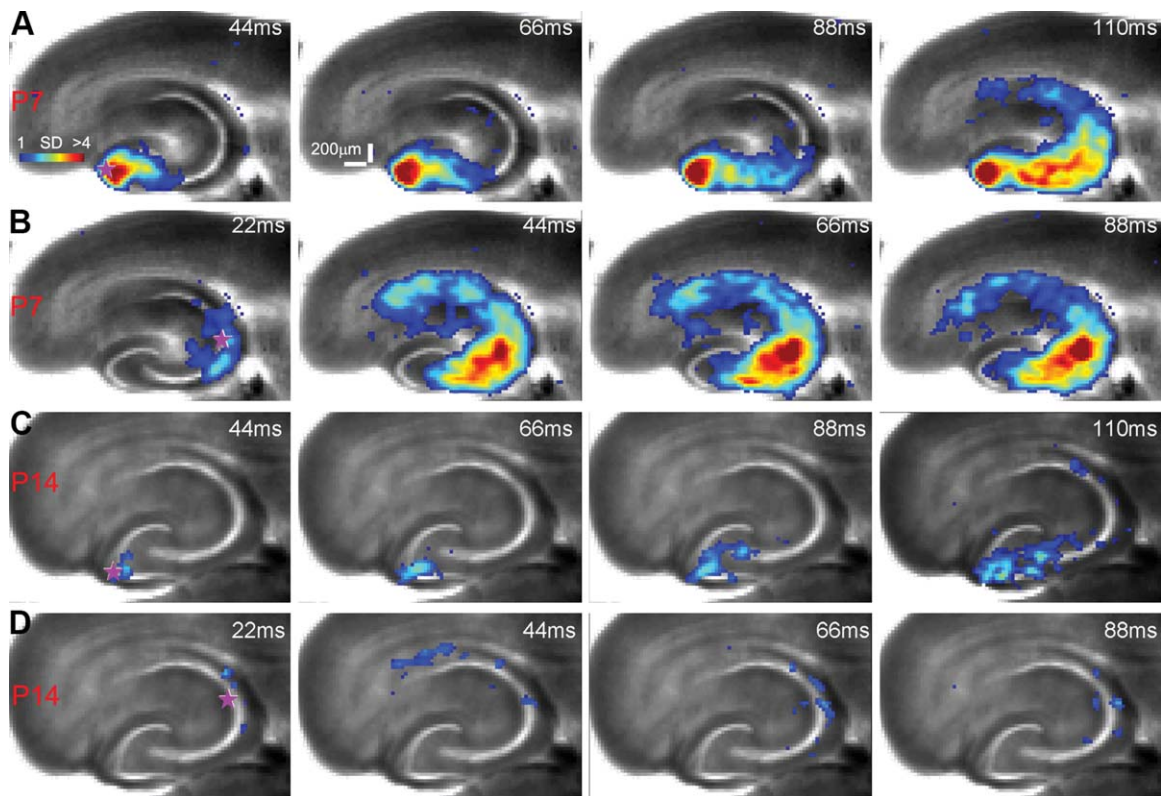
Figure 11. The emergence of the unidirectional circuit organization in the developing hippocampus occurs at about the end of the second postnatal week. **A,B:** Time series data of imaging photostimulation-evoked network activity by glutamate uncaging in DG and distal CA3 in a P7 slice, respectively. The uncaging site is denoted by a purple star. **C,D:** Time series data of imaging photostimulation-evoked network activity by glutamate uncaging in DG and distal CA3 in a P14 slice, respectively. Note that photostimulation and imaging of both slices were performed through a 2× objective and that three trials of imaging data were averaged for the presentation. Given the lower sensitivity of the 2× objective, the weaker activated granule cell layer of DG does not show as well as hilar activation in the frames presented in B, but it is detected with our signal analysis.

hippocampus by using a suite of new technologies. Fast VSD imaging allows for a macroscopic network-level view of the spatial and temporal dynamics of neural activity across the entire hippocampal circuitry. VSD signal is closely correlated with subthreshold membrane potential depolarization (rather than action potentials), so that VSD imaging is better suited to examine long-duration membrane potential depolarizations and can better reveal early neuronal activity ($\leq$P4) without fully developed action potentials compared with Ca^{2+} imaging. We corroborated our findings on spontaneous GNA in a parallel set of studies using evoked population activity by LSPS via glutamate or GABA uncaging in the developing circuitry. The LSPS approach with whole-cell recordings has furthermore provided definitive data to reveal changes in local-circuit connections over the GNA active time course.

Spontaneous hippocampal network activity

Compared with the unidirectional nature of signal propagation exhibited by the adult hippocampus, the immature hippocampal circuitry shows substantial bidirectional signal propagation, which we term *GNA*. Mouse GNA shares some features with GDP-related activity propagation and SPWs with multisite extracellular recordings (Csicsvari et al., 2000; Leinekugel et al., 1998; Maier et al., 2003). The distal CA3 origin of GNA and SPWs may be significant, in that this region is adjacent to CA2 and receives strong input from the supramammillary nucleus that has been implicated in controlling the frequency of the theta rhythm and the spread of epileptic activity in the hippocampus (Chevaleyre and Siegelbaum, 2010; Lein et al., 2005; Ochiishi et al., 1999).

Given the intrinsically bursting properties and high excitability of CA3 excitatory neurons (as we have observed), it is likely that the initiation of mouse GNA is through the intrinsic pacemaker properties of CA3 excitatory neurons and the interactions between excitatory neurons, as proposed for the hippocampus and neocortex (Sanchez-Vives et al., 2000; Sipila et al., 2005).

We have used single-cell and field potential record-ings to address the relationship among single-cell behavior, local-circuit events, and GNA. Although there is a strong correlation between the electrophysiological equivalent of GDPs in the mouse hippocampus and local field events, our results indicate that spontaneous occurrences of single-cell events like GDPs do not have a one-to-one correspondence to large-scale propagating events. This finding is consistent with the previous observation that rat GDPs can occur in the absence of local network events detected by field recordings (Sipila et al., 2005).

Mouse GNA and rat GDPs have a similar develop-mental time course; the disappearance of GNA immedi-ately transitions to the emergence of the adult-like unidirectional-circuit organization at about 2 weeks of age in the mouse. In contrast to the typical notion of GABA-mediated rat GDPs, mouse GNA, and the electro-physiological equivalent of GDPs in mouse hippocampus are largely GABA independent and mediated instead by glutamatergic transmission via AMPA receptors postna-tally. There is an interesting suggestion that glutamater-gic signaling developmentally interacts with GABAergic signaling in rat GDPs (Ben-Ari et al., 1997; Lamsa et al., 2000). In fact, it has been reported that, in neonatal rat hippocampal slices, glutamate controls the induction of GABA-mediated GDPs through AMPA receptors, and superfusion of CNQX blocks GDPs (Bolea et al., 1999). Furthermore, evoked GDPs in immature rat slices (P2–P12) are blocked in the presence of bicuculline, but GDPs evoked by suprathreshold stimuli are mostly resistant to bicuculline and inhibited with CNQX (Xie et al., 1994). Therefore, there are glutamatergic contri-butions to both mouse GNA and rat GDPs, which show differential features that may be related to species differences.

GNA and circuit maturation

In terms of functional significance, GNA may play an important role in patterning and strengthening intrahip-pocampal synaptic connections during early develop-ment, resembling other forms of spontaneous neural activity. Although the adult form of SPWs induced in slice preparations is reported to modulate synaptic con-nectivity and strength between neurons and regions (Behrens et al., 2005), correlated bursts of activity in the neonatal hippocampus in vivo (i.e., early form of SPWs) can provide correlated activity for immature neu-rons and may underlie activity-dependent maturation of the hippocampal network (Leinekugel et al., 2002). The best demonstration of the causal relationship between spontaneous network activity and synaptic input strength of specific neurons was shown experimentally

by reducing spontaneous network activity in ovo in the intact chick embryo (Gonzalez-Islas and Wenner, 2006). The forward and backward propagation of GNA could contribute to the establishment of neuronal population connections between hippocampal subfields, e.g., between CA3 and DG as well as between CA3 and CA1, through recurring local synchronous activity. We show the time course of developmentally enhanced syn-aptic connections between DG and CA3 neurons by photostimulation mapping of circuit connections to sin-gle CA3 neurons.

Our data show that the weakening and disappearance of bidirectional GNA concurs with the maturity of the tri-synaptic circuitry in which the CA3 back-propagation is reduced through decreased circuit excitability and enhanced inhibitory neuronal control that ensures unidir-ectional information flow. The most important contribut-ing factors include the maturing of the $GABA_A$ receptors and changing of circuit connectivity. We speculate that failure to control the back-propagation of distal CA3 beyond early developmental stages may contribute to pathological conditions related to learning and memory deficits and temporal lobe epileptogenesis (Myers and Scharfman, 2011; Scharfman, 2007).

In conclusion, spontaneous GNA immediately precedes the more restricted unidirectional propagation of excita-tion through the hippocampus that persists into adult-hood. Further studies that manipulate the spatial and temporal properties of GNA should reveal its functional importance for setting up the adult circuit architecture.

ROLE OF AUTHORS

Conducted experiments: YS, TI, NDO. Performed data analysis: XX, YS. Designed the experiments, supervised the project, and wrote the manuscript: XX.

CONFLICT OF INTEREST STATEMENT

We declare no competing financial interests.

LITERATURE CITED

Behrens CJ, van den Boom LP, de Hoz L, Friedman A, Heinemann U. 2005. Induction of sharp wave-ripple com-plexes in vitro and reorganization of hippocampal net-works. Nat Neurosci 8:1560–1567.

Ben-Ari Y. 2002. Excitatory actions of gaba during develop-ment: the nature of the nurture. Nat Rev Neurosci 3: 728–739.

Ben-Ari Y, Cherubini E, Corradetti R, Gaiarsa JL. 1989. Giant synaptic potentials in immature rat CA3 hippocampal neurones. J Physiol 416:303–325.

Ben-Ari Y, Khazipov R, Leinekugel X, Caillard O, Gaiarsa JL. 1997. GABA_A, NMDA and AMPA receptors: a developmentally regulated "menage a trois." Trends Neurosci 20:523–529.

Ben-Ari Y, Gaiarsa JL, Tyzio R, Khazipov R. 2007. GABA: a pioneer transmitter that excites immature neurons and generates primitive oscillations. Physiol Rev 87:1215–1284.

Bischofberger J, Engel D, Li L, Geiger JR, Jonas P. 2006. Patch-clamp recording from mossy fiber terminals in hippocampal slices. Nat Protoc 1:2075–2081.

Bolea S, Avignone E, Berretta N, Sanchez-Andres JV, Cherubini E. 1999. Glutamate controls the induction of GABA-mediated giant depolarizing potentials through AMPA receptors in neonatal rat hippocampal slices. J Neurophysiol 81:2095–2102.

Bolea S, Sanchez-Andres JV, Huang X, Wu JY. 2006. Initiation and propagation of neuronal coactivation in the developing hippocampus. J Neurophysiol 95:552–561.

Bonifazi P, Goldin M, Picardo MA, Jorquera I, Cattani A, Bianconi G, Represa A, Ben-Ari Y, Cossart R. 2009. GABAergic hub neurons orchestrate synchrony in developing hippocampal networks. Science 326:1419–1424.

Brivanlou IH, Dantzker JL, Stevens CF, Callaway EM. 2004. Topographic specificity of functional connections from hippocampal CA3 to CA1. Proc Natl Acad Sci U S A 101:2560–2565.

Buhl DL, Buzsaki G. 2005. Developmental emergence of hippocampal fast-field "ripple" oscillations in the behaving rat pups. Neuroscience 134:1423–1430.

Buzsaki G. 1986. Hippocampal sharp waves: their origin and significance. Brain Res 398:242–252.

Chevaleyre V, Siegelbaum SA. 2010. Strong CA2 pyramidal neuron synapses define a powerful disynaptic cortico-hippocampal loop. Neuron 66:560–572.

Csicsvari J, Hirase H, Mamiya A, Buzsaki G. 2000. Ensemble patterns of hippocampal CA3–CA1 neurons during sharp wave-associated population events. Neuron 28:585–594.

Dantzker JL, Callaway EM. 2000. Laminar sources of synaptic input to cortical inhibitory interneurons and pyramidal neurons. Nat Neurosci 3:701–707.

Garaschuk O, Hanse E, Konnerth A. 1998. Developmental profile and synaptic origin of early network oscillations in the CA1 region of rat neonatal hippocampus. J Physiol 507:219–236.

Gonzalez-Islas C, Wenner P. 2006. Spontaneous network activity in the embryonic spinal cord regulates AMPAergic and GABAergic synaptic strength. Neuron 49:563–575.

Grove EA, Tole S. 1999. Patterning events and specification signals in the developing hippocampus. Cereb Cortex 9:551–561.

Ikrar T, Olivas ND, Shi Y, Xu X. 2011. Mapping inhibitory neuronal circuits by laser scanning photostimulation. J Vis Exp e3109.

Ishizuka N, Weber J, Amaral DG. 1990. Organization of intrahippocampal projections originating from CA3 pyramidal cells in the rat. J Comp Neurol 295:580–623.

Lamsa K, Palva JM, Ruusuvuori E, Kaila K, Taira T. 2000. Synaptic GABA(A) activation inhibits AMPA-kainate receptor-mediated bursting in the newborn (P0–P2) rat hippocampus. J Neurophysiol 83:359–366.

Lein ES, Callaway EM, Albright TD, Gage FH. 2005. Redefining the boundaries of the hippocampal CA2 subfield in the mouse using gene expression and 3-dimensional reconstruction. J Comp Neurol 485:1–10.

Leinekugel X, Medina I, Khalilov I, Ben-Ari Y, Khazipov R. 1997. Ca2+ oscillations mediated by the synergistic excitatory actions of GABAA and NMDA receptors in the neonatal hippocampus. Neuron 18:243–255.

Leinekugel X, Khalilov I, Ben-Ari Y, Khazipov R. 1998. Giant depolarizing potentials: the septal pole of the hippocampus paces the activity of the developing intact septohippocampal complex in vitro. J Neurosci 18:6349–6357.

Leinekugel X, Khazipov R, Cannon R, Hirase H, Ben-Ari Y, Buzsaki G. 2002. Correlated bursts of activity in the neonatal hippocampus in vivo. Science 296:2049–2052.

Lorente de Nó R. 1934. Studies on the structure of the cerebral cortex. II. Continuation of the study of the ammonic system. Journal of Psychological Neurology 46:113–117.

Maier N, Nimmrich V, Draguhn A. 2003. Cellular and network mechanisms underlying spontaneous sharp wave-ripple complexes in mouse hippocampal slices. J Physiol 550:873–887.

Myers CE, Scharfman HE. 2011. Pattern separation in the dentate gyrus: a role for the CA3 backprojection. Hippocampus 21:1190–1215.

Ochiishi T, Saitoh Y, Yukawa A, Saji M, Ren Y, Shirao T, Miyamoto H, Nakata H, Sekino Y. 1999. High level of adenosine A1 receptor-like immunoreactivity in the CA2/CA3a region of the adult rat hippocampus. Neuroscience 93:955–967.

Paxinos G, Franklin KBJ. 2001. The mouse brain in stereotaxic coordinates. San Diego: Academic Press.

Sanchez-Vives MV, Nowak LG, McCormick DA. 2000. Membrane mechanisms underlying contrast adaptation in cat area 17 in vivo. J Neurosci 20:4267–4285.

Scharfman HE. 1994. EPSPs of dentate gyrus granule cells during epileptiform bursts of dentate hilar "mossy" cells and area CA3 pyramidal cells in disinhibited rat hippocampal slices. J Neurosci 14:6041–6057.

Scharfman HE. 2007. The CA3 "backprojection" to the dentate gyrus. Prog Brain Res 163:627–637.

Shepherd GM, Stepanyants A, Bureau I, Chklovskii D, Svoboda K. 2005. Geometric and functional organization of cortical circuits. Nat Neurosci 8:782–790.

Shi Y, Nenadic Z, Xu X. 2010. Novel use of matched filtering for synaptic event detection and extraction. PLoS One 5:e15517.

Sipila ST, Huttu K, Soltesz I, Voipio J, Kaila K. 2005. Depolarizing GABA acts on intrinsically bursting pyramidal neurons to drive giant depolarizing potentials in the immature hippocampus. J Neurosci 25:5280–5289.

Tole S, Christian C, Grove EA. 1997. Early specification and autonomous development of cortical fields in the mouse hippocampus. Development 124:4959–4970.

Weiler N, Wood L, Yu J, Solla SA, Shepherd GM. 2008. Top-down laminar organization of the excitatory network in motor cortex. Nat Neurosci 11:360–366.

Xie X, Hider RC, Smart TG. 1994. Modulation of GABA-mediated synaptic transmission by endogenous zinc in the immature rat hippocampus in vitro. J Physiol 478:75–86.

Xu X, Callaway EM. 2009. Laminar specificity of functional input to distinct types of inhibitory cortical neurons. J Neurosci 29:70–85.

Xu X, Olivas ND, Levi R, Ikrar T, Nenadic Z. 2010. High precision and fast functional mapping of cortical circuitry through a combination of voltage sensitive dye imaging and laser scanning photostimulation. J Neurophysiol 103:2301–2312.